Preparation of Nanoporous Ruthenium Catalyst and Its CO Oxidation Characteristics

Hakamada, Masataka; Motomura, Junichi; Hirashima, Fumi; Mabuchi, Mamoru

Materials Transactions, Vol. 53, No. 3 (2012) pp. 524 to 530

Preparation of Nanoporous Ruthenium Catalyst and Its CO Oxidation Characteristics

Masataka Hakamada, Junichi Motomura*, Fumi Hirashima* and Mamoru Mabuchi

Department of Energy Science and Technology, Graduate School of Energy Science, Kyoto University, Kyoto 606-8501, Japan

Anodic polarization measurements for various ruthenium (Ru) alloys revealed that hexagonal close-packed nanoporous Ru (np-Ru) can be fabricated by dealloying or selective dissolution of manganese (Mn) from Ru–Mn alloy. The pore size and specific surface area of fabricated np-Ru were 3 nm and 51.5 $m^2 g^{-1}$, respectively. An electron diffraction pattern suggested a polycrystalline nature of the fabricated np-Ru, which is perhaps due to the change in the crystal structure during dealloying. The oxidation of carbon monoxide (CO) was efficiently catalyzed by the np-Ru. The activation energy was 82 kJ mol^{-1} which is comparable to that of the polycrystalline RuO_2/Ru catalyst. The present np-Ru is a novel candidate as a recoverable Ru catalyst. [doi:10.2320/matertrans.M2011326]

(Received October 24, 2011; Accepted December 16, 2011; Published February 8, 2012)

Keywords: *ruthenium, catalyst, porous materials, dealloying, CO oxidation*

1. Introduction

Ruthenium (Ru) is one of the less-expensive platinum-group metals (PGM), and is known for its unique catalytic oxidation of carbon monoxide (CO) to carbon dioxide ($CO + 1/2O_2 \rightarrow CO_2$). While Ru is the poorest PGM catalyst for CO oxidation under ultrahigh vacuum,[1] it is a superior catalyst under ambient pressure.[2,3] This "pressure gap" is only observed for Ru, and was once attributed to RuO_2 formation at the surface.[4] However, more recent studies suggest that this behavior can be rationalized in terms of CO and oxygen binding,[5] and its exact origin is still being debated. Joo *et al.* reported that Ru nanoparticles with diameters of 2–6 nm exhibited inverse size dependence in catalyzing the oxidation of CO.[6] Larger nanoparticles exhibited a higher conversion, despite their specific surface area being smaller. These results suggest that CO oxidation by these less-expensive Ru catalysts has the potential for investigation and promotion in practical applications. For example, the purification of automobile exhaust gases and the selective oxidation of fuel streams for polymer electrolyte fuel cells are attractive potential applications.

Studies of CO oxidation by Ru catalysts have predominantly been conducted using Ru single crystal faces.[1,2,4,5,7,8] Supported Ru nanoparticles have been also used in catalytic studies.[3,6,9–11] Unsupported porous-metallic catalysts are another promising form of catalyst. Porous-metallic catalysts are superior to supported nanoparticle catalysts in terms of recovery after use, because the separation of catalytic metals from the porous skeletal support is unnecessary for porous-metallic catalysts. In addition to conventional Raney Ni or Cu porous catalysts,[12,13] nanoporous metals fabricated by dealloying[14] are emerging potential catalysts. Nanoporous Au fabricated by dealloying of Au–Ag alloys exhibits catalytic activity for CO oxidation,[15,16] in contrast to bulk Au. Nanoporous Pt exhibits abnormal hydrogen sorption characteristics, probably due to surface lattice disorder.[17] Thus, nanoporous metal structure appears to influence various phenomena within the nanopores. CO oxidation over unsupported nanoporous Ru (np-Ru) is also worth investigating, however the fabrication and catalytic properties of np-Ru have been much less frequently documented. Aika *et al.* thoroughly elucidated the catalytic properties of porous Raney Ru fabricated by dealloying of Ru–Al alloys in alkaline solution,[18–23] although CO oxidation over Raney Ru has not been reported to date. Xu *et al.* investigated the electrocatalytic properties of nanoporous Pt–Ru synthesized from a Pt–Ru–Al ternary starting alloy.[24] Ru–Al starting alloys inevitably possess intermetallic compounds,[25,26] which leads to heterogeneity in the resulting structure. A single-phase solid solution of Ru alloy is a more suitable starting material for np-Ru with a homogeneous nanostructure.

In this study, the anodic polarization behavior of Ru-containing single-phase alloys in an electrolyte was examined, for fabrication of np-Ru by dealloying. Very fine nanoporous structures with typical lengths of 3 nm were generated in hexagonal close-packed (hcp) metallic Ru. The catalytic activity of fabricated np-Ru for CO oxidation was then investigated to determine the activation energy (E_a) of the reaction.

2. Experimental

2.1 Electrochemical examination for fabrication of np-Ru

To determine a suitable starting alloy for np-Ru, commercially available Ru (powder, >99.9%) was alloyed with various sacrificial elements. Co (lumps, 99.9%), Fe (grains, 99.9%), Mn (grains, 99.9%), Ni (grains, >99.9%), Cr (grains, 99.9%) and Ti (plate, 99.5%) were prepared as potential sacrificial elements. Their standard electrode potentials are sufficiently lower than that of Ru.[27] Ingots of $Ru_{0.20}Co_{0.80}$, $Ru_{0.20}Fe_{0.80}$, $Ru_{0.20}Mn_{0.80}$, $Ru_{0.20}Ni_{0.80}$, $Ru_{0.16}Cr_{0.84}$ and $Ru_{0.16}Ti_{0.84}$, all of which are single-phase solid solution alloys,[28] were fabricated by arc melting under an Ar atmosphere and subsequent homogenization annealing at 1473 K ($Ru_{0.20}Ni_{0.80}$, $Ru_{0.20}Fe_{0.80}$), 1273 K ($Ru_{0.20}Mn_{0.80}$), 1173 K ($Ru_{0.20}Co_{0.80}$) or 873 K ($Ru_{0.16}Cr_{0.84}$, $Ru_{0.16}Ti_{0.84}$) for 24 h in an Ar + 5% H_2 atmosphere.

*Graduate Student, Kyoto University

The quasi-static electrochemical behavior of the alloy ingots was examined by linear sweep voltammetry in 0.1 mol/L H_2SO_4 electrolyte with a scan rate of 1 mV s^{-1}, using a standard three-electrode electrochemical cell with a Pt wire as a counter electrode, a saturated calomel electrode (SCE) as a reference electrode and the alloy (polished with #1200 SiC paper) as a working electrode. A 9 mm^2 area of the working electrode was exposed to the electrolyte by covering the rest of the alloy surface with Teflon tape.

According to the anodic polarization behaviors of the Ru alloys, $Ru_{0.20}Mn_{0.80}$ alloy was subjected to dealloying to fabricate np-Ru. A constant electrochemical potential of +700 mV (vs SCE) was applied to the $Ru_{0.20}Mn_{0.80}$ working electrode for 5 h at room temperature.

Scanning electron microscopy (SEM) images of samples were recorded using SU6600 (Hitachi High-Technologies Corp.) at an accelerating voltage of 20 kV. During the SEM observation, energy-dispersive X-ray spectroscopy (EDXS) was also conducted for elemental analyses. Samples for transmission electron microscopy (TEM) observation were prepared using an ion-slicing apparatus after mounting sample powder in an epoxy resin. TEM images were recorded using a JEM-2100F microscope (JEOL Ltd.) at an operating voltage of 200 kV. X-ray diffraction (XRD) analyses were performed using X'Pert Pro (PANalytical) with Cu-Kα radiation. N_2 adsorption/desorption isotherms of the sample pretreated at 383 K for 3 h in vacuum was obtained using AUTOSORB-1-C (Quantachrome Instruments). X-ray photoelectron spectroscopy (XPS) was also conducted on the np-Ru under vacuum (6.7×10^{-8} Pa) using ULVAC-PHI ESCA5800 with Al Kα radiation ($h\nu = 1486.6$ eV) for surface analyses.

2.2 Catalytic activity for CO oxidation

To examine the catalytic activity of np-Ru, CO oxidation reactions in the presence of np-Ru were carried out. 14 mg of dealloyed np-Ru was ground and supported with quartz wool in a 4 mm internal diameter Pyrex reaction tube. The reactor was placed in a heater bag where the temperature was measured and controlled using a K-type thermocouple close to the 0.8 mm thick catalyst layer. A N_2 balanced mixture gas containing 4% CO and 2% O_2 was introduced in the tube at a flow rate of 50 ml min^{-1} (space velocity = 3.1×10^5 h^{-1}). The CO conversion rate at 298–423 K was measured by gas chromatography [Shimadzu GC-8AIT with molecular sieve 5A (60–80)] of the product gas. The turnover frequency (TOF) was calculated from the CO conversion rate using a Ru atomic surface area value of 8.6 $Å^2$ [29] using following equation:

$$\mathrm{TOF} = \frac{\text{Number of reacted CO molecule per second}}{\text{Number of atoms at surface of np-Ru}} = \frac{\text{Gas flow rate} \times \text{CO concentration in initial gas} \times \text{number of molecules in unit volume} \times \text{CO conversion rate}}{\text{specific surface area of sample} \times \text{sample mass/atomic surface area of Ru}}. \quad (1)$$

No preheating treatment was conducted, because the nanoporous structure was maintained even after CO oxidation at 399 K (confirmed by SEM observations) and no substantial structural changes in np-Ru occurred during CO oxidation. For comparison, catalytic activity of commercially available Ru powder (particle diameter < 400 µm, purchased from The Nilaco Corp.) was also examined in a similar manner.

3. Results and Discussion

3.1 Fabrication of np-Ru

Preliminary XRD and EDXS analyses suggested that the initial alloy ingots had uniform composition and crystal structure without surface segregation of elemental metallic Ru. Anodic polarization curves of the Ru alloys are shown in Fig. 1, with the curves of the pure sacrificial elements also shown for comparison. Pure elemental Co, Fe and Ni exhibited an increase in current with anodic potential sweep. When these metals were alloyed with Ru, only very small currents were detected [Figs. 1(a), 1(b) and 1(d)], meaning that no dissolution of Co, Fe and Ni from the alloys occurred in the electrolyte. Very little current was detected during the anodic polarization of pure Cr, pure Ti, $Ru_{0.16}Cr_{0.84}$ and $Ru_{0.16}Ti_{0.84}$ in the electrolyte [Figs. 1(e) and 1(f)]. Cr and Ti appeared to form oxide surface films which passivate dissolution into the electrolyte. In contrast, pure Mn and $Ru_{0.20}Mn_{0.80}$ alloy showed clear increasing responses to potential sweeping [Fig. 1(c)], which suggested that Mn readily dissolved into H_2SO_4 from both the $Ru_{0.20}Mn_{0.80}$ alloy and pure Mn. The monotonic increase in current indicates the evolution of porosity, by the dissolution and aggregation of less and more noble elements, respectively.[14,30,31] Thus, Mn is a promising sacrificial element for the fabrication of np-Ru.

Figure 2 shows the current transition during electrolysis using $Ru_{0.20}Mn_{0.80}$ alloy as a working electrode in 0.1 mol/L H_2SO_4 at a constant potential of +700 mV vs SCE. A large current was observed during the initial stage of electrolysis, followed by a gradual decrease to a negligible level. This transition is similar to the dealloying of Au–Ag alloy to fabricate nanoporous Au.[32] After electrolysis, the working electrode had become brittle and was washed with distilled water and allowed to dry. During the recovery, washing and drying operation, the sample became powdery.

Microstructure observations and analyses of the sample are shown in Figs. 3 and 4, respectively, and revealed that np-Ru had been fabricated by dealloying of $Ru_{0.20}Mn_{0.80}$. TEM observations of the sample in Figs. 3(a) and 3(b) showed a nanoporous structure with typical pore and ligament sizes of approximately 3 nm, although the overlap of ligaments made the precise measurement of these sizes difficult. To obtain clearer evidence of the nanoporous structure by the coarsening of pores and ligaments,[33] the dealloyed sample was annealed at 773 K for 5 h and at 1273 K for 2 h under an Ar + 5%H_2 atmosphere. SEM observations of dealloyed and annealed samples are shown in Figs. 3(d)–3(f). The annealed

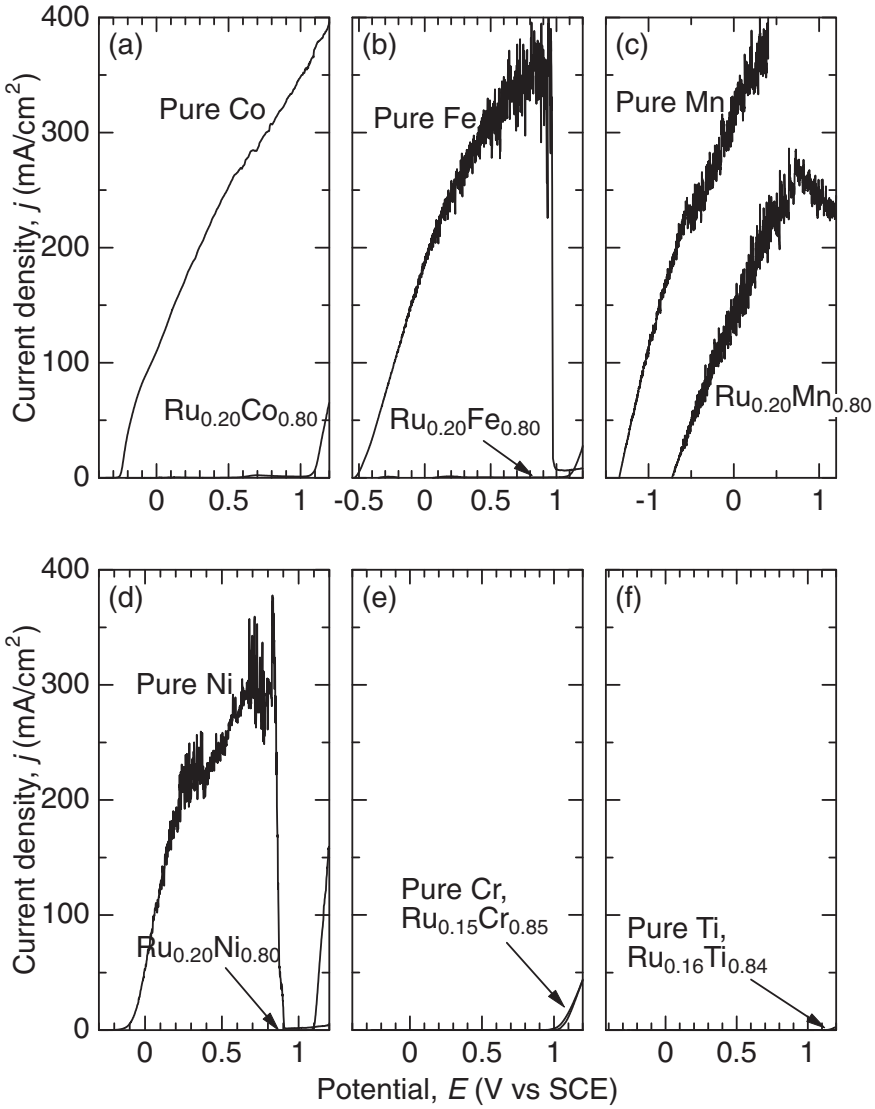

Fig. 1 Anodic polarization curves in 0.1 mol/L H_2SO_4 for (a) pure Co and $Ru_{0.20}Co_{0.80}$, (b) pure Fe and $Ru_{0.20}Fe_{0.80}$, (c) pure Mn and $Ru_{0.20}Mn_{0.80}$, (d) pure Ni and $Ru_{0.20}Ni_{0.80}$, (e) pure Cr and $Ru_{0.16}Cr_{0.84}$ and (f) pure Ti and $Ru_{0.16}Ti_{0.84}$.

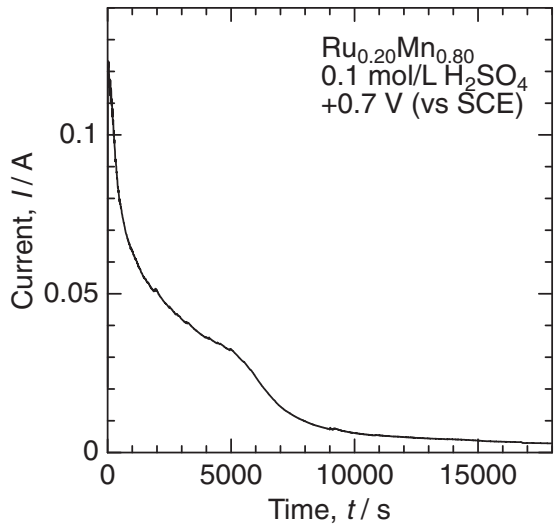

Fig. 2 Current transition during dealloying of $Ru_{0.20}Mn_{0.80}$ in 0.1 mol/L H_2SO_4.

sample exhibited a clear nanoporous structure with ligaments and pores of 200 nm (when annealed at 773 K) and 700 nm (when annealed at 1273 K) in size. The coarsening of the nanoporous structure is similar to that reported for other nanoporous metals including Au,[34] Pt[33] and Pd.[35] XRD patterns of the sample showed broad peaks characteristic of metallic Ru with a hcp structure, as shown in Fig. 4(a). EDXS showed that the major component of the sample was Ru, and that trace Mn (<10 at%) remained after electrolysis [Fig. 4(b)].

N_2 adsorption/desorption isotherms and the pore size distribution calculated from the Barrett–Joyner–Halenda (BJH) approach are shown in Fig. 5. The isotherms [Fig. 5(a)] indicated that the specific surface area of np-Ru was 51.5 $m^2 g^{-1}$, using the multipoint Brunauer–Emmett–Teller (BET) approach. This value is comparable with those of conventional nanoparticulate[36] and nanoporous[37] oxide supports. Calculations based on the isotherms revealed that the volumetric porosity and average pore size of np-Ru were 37% and 3.2 nm, respectively. These parameters are in good

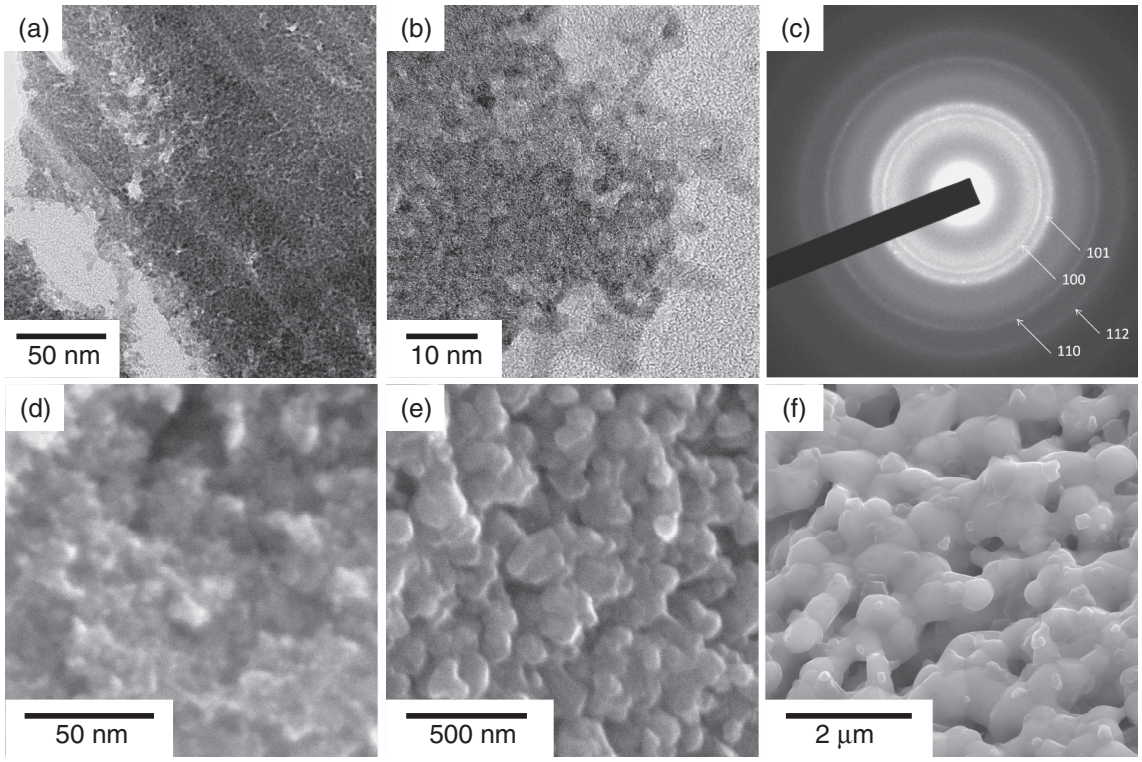

Fig. 3 TEM (a), (b), SAED pattern (c) and SEM (d)–(f) images of np-Ru fabricated by dealloying of $Ru_{0.20}Mn_{0.80}$. Samples in (a)–(d) were as-dealloyed samples, while those in (d) and (e) were annealed at 773 K for 5 h and 1273 K for 2 h, respectively.

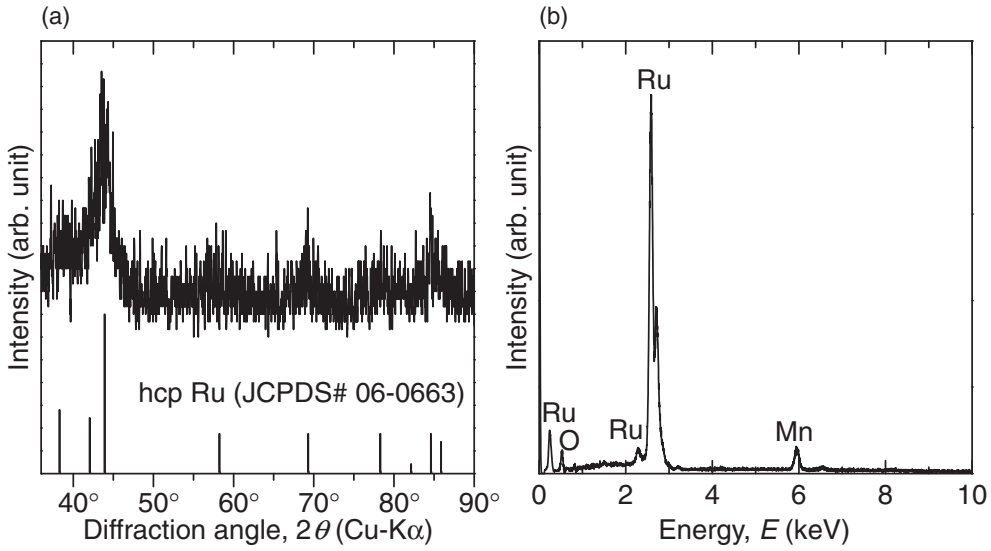

Fig. 4 (a) XRD pattern and (b) EDX spectrum of np-Ru fabricated by dealloying of $Ru_{0.20}Mn_{0.80}$.

agreement with those estimated from TEM observations [Figs. 3(a) and 3(b)]. Thus, np-Ru possessed a high specific surface area.

A selected area electron diffraction (SAED) pattern [Fig. 3(c)] detected from the 350 nm diameter region suggested a polycrystalline nature of the fabricated np-Ru. The broadening of XRD peaks [Fig. 4(a)] suggested that the crystallite size of np-Ru was approximately 3 nm according to Scherrer's equation, (although the strict evaluation is difficult due to low intensity), while the starting $Ru_{0.20}Mn_{0.80}$ alloy had a crystallite size in the order of micrometers (indicated by the sharp XRD peak for $Ru_{0.20}Mn_{0.80}$, as shown in Fig. 6). These results, together with the TEM images and pore size estimation, indicated that the crystallite size was similar to the ligament and pore sizes in np-Ru. This situation is different from that in the dealloying of Au–Ag to fabricate nanoporous Au, where the crystallite size is retained during nanoporosity formation and is typically much larger than ligament and pore sizes.[38] It is known and also confirmed by XRD analyses in this study (Figs. 4(a) and 6), that $Ru_{0.20}Mn_{0.80}$ alloy has a face-centered-cubic (fcc) crystal structure,[28,39] while pure metallic Ru has a hcp structure.

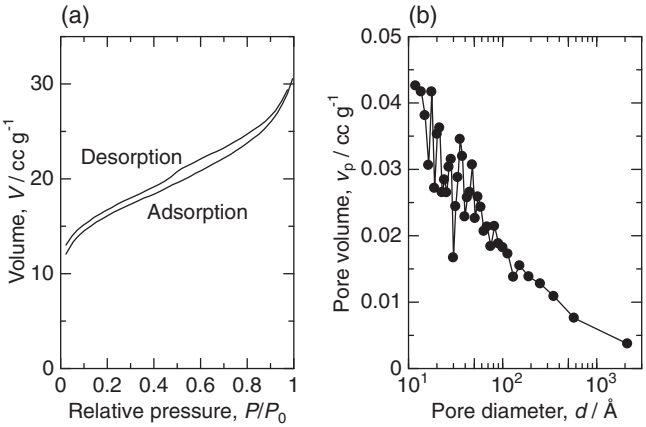

Fig. 5 (a) N_2 adsorption–desorption isotherms and (b) calculated pore size distribution of np-Ru fabricated by dealloying of $Ru_{0.20}Mn_{0.80}$.

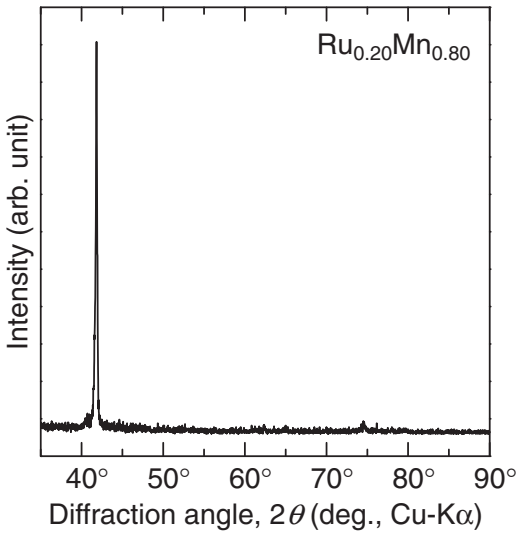

Fig. 6 XRD pattern of $Ru_{0.20}Mn_{0.80}$. The diffraction at 42° indicated that the sample contained a solid solution of face-centered-cubic (fcc) Ru–Mn alloy, since the strongest diffractions for fcc Ru(111) and Mn(111) are observed at 40.8 and 44.9°, respectively. The sharpness of the diffraction indicated that the crystallite size of the initial $Ru_{0.20}Mn_{0.80}$ alloy was in the micrometer-millimeter range, while the crystallite size of nanoporous Ru (np-Ru) after dealloying was in the nanometer range.

Thus, the crystal structure changed from fcc to hcp during the dealloying of $Ru_{0.20}Mn_{0.80}$. Yu *et al.*[40] reported that amorphous $Pd_{0.3}Ni_{0.5}P_{0.2}$ can be dealloyed to fabricate crystalline nanoporous Pd whose crystallite size is similar to its ligament size. Thus, changes in crystal structure may result in polycrystalline ligaments in nanoporous metals fabricated by dealloying.

In addition to dealloying under electrochemical potential in H_2SO_4, free corrosion (the simple immersion in electrolytes without electrochemical potential) of $Ru_{0.20}Mn_{0.80}$ in 0.1 mol/L H_2SO_4 and 1 mol/L $(NH_4)_2SO_4$ electrolytes was carried out at room temperature. Additional SEM observations and XRD analyses confirmed that both free corrosion experiments resulted in the synthesis of np-Ru with single-nanometer-sized pores. Thus, Ru–Mn alloy is a promising starting material for the efficient production of np-Ru catalysts.

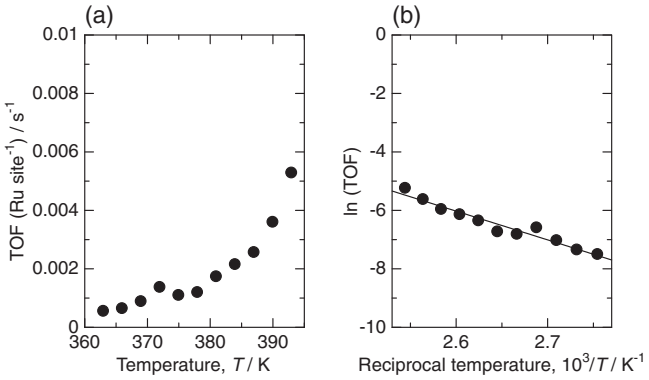

Fig. 7 (a) Change in turnover frequency (TOF) with temperature and (b) arrhenius plots for CO oxidation over np-Ru catalyst.

3.2 Catalytic activity for CO oxidation

The relationship between reaction temperature and TOF, where CO conversion is less than 10%, is shown in Fig. 7(a). As the reaction temperature increased, more CO reacted in the presence of the np-Ru catalyst. At temperature above 396 K, almost all CO reacted. On the other hand, commercially available Ru powder showed no catalytic activity on CO oxidation at temperatures below 399 K. Arrhenius plots for the CO oxidation over np-Ru are shown in Fig. 7(b). The E_a determined from the Arrhenius plots was 82 kJ mol^{-1}, and is similar to those obtained in previous CO oxidation experiments with various Ru catalysts, summarized by Assmann *et al.*[41] including single crystal Ru,[2] polycrystalline Ru[42] and supported Ru nanoparticles.[9,43]

Various factors affect the activity of catalysts, including the catalyst surface oxidation state which is crucially important for CO oxidation over Ru catalysts.[1–11,41–43] Figure 8 shows the XPS result of np-Ru, suggesting that a considerable portion of the np-Ru surface was oxidized [shoulder at 280.5–210 eV in Fig. 8(a)], although the XRD pattern in Fig. 4(a) exhibited no RuO_2 peaks. This suggests that the np-Ru surface was partly covered with a very thin active oxide layer, which may have been responsible for the np-Ru activity. However, further analyses such as *in-situ* infrared spectroscopy are required to elucidate the CO oxidation mechanism over np-Ru, because the metallic Ru surface oxidation state is very sensitive to the atmosphere.[9,10,41] On the other hand, a measurable amount of residual Mn was also detected by XPS [Fig. 8(b)], although strict elemental composition cannot be calculated due to overlap of Ru 3d and C 1s peaks, unfortunately. The majority of the peak intensity is detected above 639.0 eV corresponding to pure metallic Mn, which suggests oxidation and/or alloyed state of Mn in the np-Ru. Recent publications[44–47] show the catalytic activity of crystalline Mn oxides toward CO oxidation at low temperatures; however, crystalline Mn oxides was not detected in the present np-Ru [Fig. 4(a)]. Thus Mn oxide at the surface of np-Ru, if any, is in an amorphous state, whose catalytic activity has been not reported for CO oxidation. Furthermore, the activation energy of np-Ru was similar to previous Ru catalysts. These indicate that residual Mn has a possible but minor effect on the catalytic activity of np-Ru for CO oxidation.

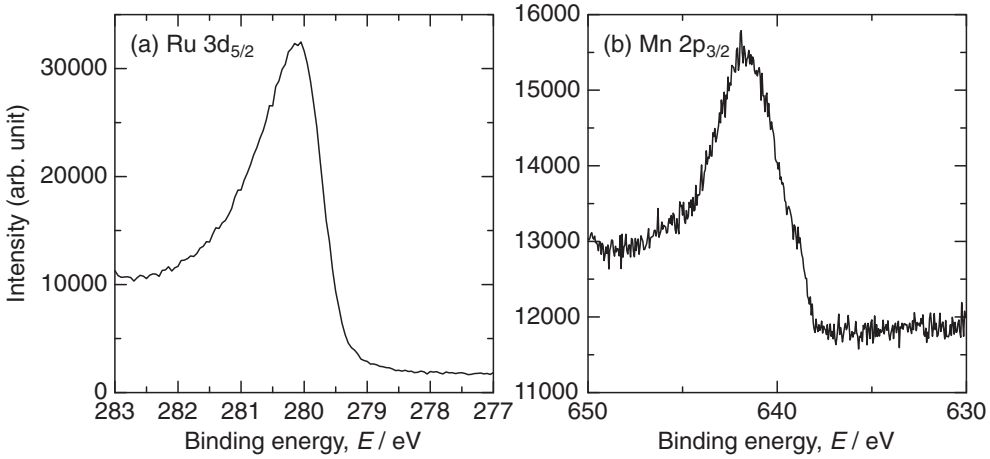

Fig. 8 XPS results for np-Ru showing peaks for (a) Ru $3d_{5/2}$ and (b) Mn $2p_{3/2}$.

4. Conclusions

In summary, anodic polarization measurements of Ru alloys with a high content of various sacrificial elements revealed that Ru–Mn alloy is a suitable starting alloy for np-Ru fabrication. Electrochemical dealloying of $Ru_{0.20}Mn_{0.80}$ resulted in Mn dissolution and the synthesis of np-Ru with pore and ligament sizes of approximately 3 nm. Synthesized np-Ru exhibited catalytic activity for CO oxidation, with an activation energy similar to those of precedent Ru catalysts. Consequently, np-Ru is a candidate as a recoverable Ru catalyst. Surface features of the nanoporous metal such as surface strain and segregation of residual elements (Mn in this case) may promote catalytic performance, for example, in Fischer-Tropsch synthesis.[48)]

Acknowledgments

M. H. thanks the Izumi Science and Technology Foundation for support for the synthesis of np-Ru. CO oxidation measurements over np-Ru were supported financially by a JSPS Grant-in-Aid for Scientific Research (C) 21605013 and technically by Dr. Y. Tai (National Institute of Advanced Industrial Science and Technology). The authors also thank Prof. T. Yao, Prof. M. Hibino and Prof. T. Yabutsuka (Kyoto Univ.) for the cooperation of SEM observations and Prof. T. Hirato and Prof. M. Miyake (Kyoto Univ.) for XRD analyses.

REFERENCES

1) H.-I. Lee and J. M. White: J. Catal. **63** (1980) 261–264.
2) C. H. F. Peden and D. W. Goodman: J. Phys. Chem. **90** (1986) 1360–1365.
3) N. W. Cant, P. C. Hicks and B. S. Lennon: J. Catal. **54** (1978) 372–383.
4) H. Over and M. Muhler: Prog. Surf. Sci. **72** (2003) 3–17.
5) F. Gao and D. W. Goodman: Langmuir **26** (2010) 16540–16551.
6) S. H. Joo, J. Y. Park, J. R. Renzas, D. R. Butcher, W. Huang and G. A. Somorjai: Nano Lett. **10** (2010) 2709–2713.
7) Y. K. Kim, G. A. Morgan, Jr. and J. Y. Yates, Jr.: J. Phys. Chem. C **111** (2007) 3366–3368.
8) D. W. Goodman, C. H. F. Peden and M. S. Chen: Surf. Sci. **601** (2007) L124–L126.
9) J. Assmann, V. Narkhede, L. Khodeir, E. Löffler, O. Hinrichsen, A. Birkner, H. Over and M. Muhler: J. Phys. Chem. B **108** (2004) 14634–14642.
10) J. Aßmann, D. Crihan, M. Knapp, E. Lundgren, E. Löffler, M. Muhler, V. Narkhede, H. Over, M. Schmid, A. P. Seitsonen and P. Varga: Angew. Chem. Int. Ed. **44** (2005) 917–920.
11) J. T. Kiss and R. D. Gonzalez: J. Phys. Chem. **88** (1984) 892–897.
12) S. Rakass, H. Oudghiri-Hassani, P. Rowntree and N. Abatzoglou: J. Power Sources **158** (2006) 485–496.
13) M. S. Wainwright and D. L. Trimm: Catal. Today **23** (1995) 29–42.
14) J. Erlebacher, M. J. Aziz, A. Karma, N. Dimitrov and K. Sieradzki: Nature **410** (2001) 450–453.
15) S. Kameoka and A. P. Tsai: Catal. Lett. **121** (2008) 337–341.
16) A. Wittstock, B. Newmann, A. Schaefer, K. Dumbuya, C. Kübel, M. M. Biener, V. Zielasek, H.-P. Steinrück, J. M. Gottfried, J. Biener, A. Hamza and M. Bäumer: J. Phys. Chem. C **113** (2009) 5593–5600.
17) M. Hakamada, T. Furukawa, T. Yamamoto, M. Takahashi and M. Mabuchi: Mater. Trans. **52** (2011) 806–809.
18) Y. Ogata, K. Aika and T. Onishi: Surf. Sci. **140** (1984) L285–L289.
19) Y. Ogata, K. Aika and T. Onishi: J. Catal. **112** (1988) 469–477.
20) K. Aika, Y. Ogata, K. Takeishi, K. Urabe and T. Onishi: J. Catal. **114** (1988) 200–205.
21) T. Hikita, Y. Kadowaki and K. Aika: J. Phys. Chem. **95** (1991) 9396–9402.
22) K. Takeishi and K. Aika: J. Catal. **136** (1992) 252–257.
23) K. Takeishi, Y. Yamashita and K. Aika: Appl. Catal. A **168** (1998) 345–351.
24) C. Xu, L. Wang, X. Mu and Y. Ding: Langmuir **26** (2010) 7437–7443.
25) S. M. Anlage, P. Nash, R. Ramachandran and R. B. Schwarz: J. Less-Common Metals **136** (1988) 237–247.
26) Z. A. Chaudhury and C. Suryanarayana: J. Mater. Sci. **17** (1982) 3158–3164.
27) M. Pourbaix: *Atlas of Electrochemical Equilibria in Aqueous Solutions*, (Pergamon Press, Oxford, 1966).
28) T. B. Massalski and H. Okamoto (eds.): *Binary Alloy Phase Diagrams*, (ASM International, Ohio, 1990).
29) P. Panagiotopoulou, D. I. Kondarides and X. E. Verykios: Appl. Catal. B **88** (2009) 470–478.
30) K. Sieradzki, N. Dimitrov, D. Movrin, C. McCall, N. Vasiljevic and J. Erlebacher: J. Electrochem. Soc. **149** (2002) B370–B377.
31) M. Hakamada, K. Tajima, K. Yoshimura, Y. Chino and M. Mabuchi: J. Alloy. Compd. **494** (2010) 309–314.
32) A. K. Mishra, C. Bansal and H. Hahn: J. Appl. Phys. **103** (2008) 094308.
33) D. V. Pugh, A. Dursun and S. G. Corcoran: J. Mater. Res. **18** (2003) 216–221.
34) R. Li and K. Sieradzki: Phys. Rev. Lett. **68** (1992) 1168–1171.
35) M. Hakamada and M. Mabuchi: J. Alloy. Compd. **479** (2009) 326–329.
36) M. Haruta, S. Tsubota, T. Kobayashi, H. Kageyama, M. J. Genet and B. Delmon: J. Catal. **144** (1993) 175–192.
37) T. Sreethawong and S. Yoshikawa: Catal. Commun. **6** (2005) 661–668.

38) S. V. Petegem, S. Brandstetter, R. Maass, A. M. Hodge, B. S. El-Dasher, J. Biener, B. Schmitt, C. Borca and H. V. Swygenhoven: Nano Lett. **9** (2009) 1158–1163.
39) J. Häglund, A. Fernández Guillermet, G. Grimvall and M. Körling: Phys. Rev. B **48** (1993) 11685–11691.
40) J. Yu, Y. Ding, C. Xu, A. Inoue, Y. Sakurai and M. Chen: Chem. Mater. **20** (2008) 4548–4550.
41) J. Assmann, V. Narkhede, N. A. Breuer, M. Muhler, A. P. Seitsonen, M. Knapp, D. Crihan, A. Farkas, G. Mellau and H. Over: J. Phys.: Condens. Matter **20** (2008) 184017.
42) J. Wang, C. Y. Fan, K. Jacobi and G. Ertl: J. Phys. Chem. B **106** (2002) 3422–3427.
43) J. Aßmann, E. Löffler, A. Birkner and M. Muhler: Catal. Today **85** (2003) 235–249.
44) S. Ching, D. A. Kriz, K. M. Luthy, E. C. Njagi and S. L. Suib: Chem. Commun. **47** (2011) 8286–8288.
45) Y.-F. Han, F. Chen, Z.-Y. Zhong, K. Ramesh, E. Widjaja and L.-W. Chen: Catal. Commun. **7** (2006) 739–744.
46) S. A. C. Carabineiro, S. S. T. Bastos, J. J. M. Órfão, M. F. R. Pereira, J. J. Delgado and J. L. Figueiredo: Catal. Lett. **134** (2010) 217–227.
47) K. Ramesh, L. Chen, F. Chen, Y. Liu, Z. Wang and Y.-F. Han: Catal. Today **131** (2008) 477–482.
48) J. Kang, K. Cheng, L. Zhang, Q. Zhang, J. Ding, W. Hua, Y. Lou, Q. Zhai and Y. Wang: Angew. Chem. Int. Ed. **50** (2011) 5200–5203.